

Movement correction in DCE-MRI through windowed and reconstruction dynamic mode decomposition

Santosh Tirunagari^{1,2}  · Norman Poh¹ · Kevin Wells² · Miroslaw Bober² · Isky Gordon³ · David Windridge⁴

Received: 26 May 2016 / Revised: 2 January 2017 / Accepted: 14 March 2017 / Published online: 6 April 2017
© The Author(s) 2017. This article is an open access publication

Abstract Images of the kidneys using dynamic contrast-enhanced magnetic resonance renography (DCE-MRR) contains unwanted complex organ motion due to respiration. This gives rise to motion artefacts that hinder the clinical assessment of kidney function. However, due to the rapid change in contrast agent within the DCE-MR image sequence, commonly used intensity-based image registration techniques are likely to fail. While semi-automated approaches involving human experts are a possible alternative, they pose significant drawbacks including inter-observer variability, and the bottleneck introduced through manual

inspection of the multiplicity of images produced during a DCE-MRR study. To address this issue, we present a novel automated, registration-free movement correction approach based on windowed and reconstruction variants of dynamic mode decomposition (WR-DMD). Our proposed method is validated on ten different healthy volunteers' kidney DCE-MRI data sets. The results, using block-matching-block evaluation on the image sequence produced by WR-DMD, show the elimination of 99% of mean motion magnitude when compared to the original data sets, thereby demonstrating the viability of automatic movement correction using WR-DMD.

Santosh Tirunagari and Norman Poh have benefited from the Medical Research Council (MRC) funded project 'Modelling the Progression of Chronic Kidney Disease' under the grant number R/M023281/1.

Electronic supplementary material The online version of this article (doi:[10.1007/s00138-017-0835-5](https://doi.org/10.1007/s00138-017-0835-5)) contains supplementary material, which is available to authorized users.

✉ Santosh Tirunagari
s.tirunagari@surrey.ac.uk

Norman Poh
n.poh@surrey.ac.uk

Kevin Wells
k.wells@surrey.ac.uk

Miroslaw Bober
m.bober@surrey.ac.uk

¹ Department of Computer Science, University of Surrey, Guildford, Surrey GU2 7XH, UK

² Center for Vision, Speech and Signal Processing (CVSSP), University of Surrey, Guildford, Surrey GU2 7XH, UK

³ University College London (UCL) Institute of Child Health, 30 Guildford Street, London WC1N 1EH, UK

⁴ Department of Computer Science, Middlesex University, The Burroughs, Hendon, London NW4 4BT, UK

Keywords DMD · W-DMD · R-DMD · WR-DMD · DCE-MRI · Movement correction

1 Introduction

Dynamic contrast-enhanced magnetic resonance imaging (DCE-MRI) renography is a promising technique for functional assessment of the kidney because it avoids the need for ionising radiation. In order to obtain useful diagnostic/prognostic information, the dynamic change of pixel intensities as contrast agent flows through the metabolic region within the kidney must be quantified in terms of function such as blood flow, filtration rate or functional volume. However, absolute quantification inside the kidney is often obfuscated by complex patient movements, arising due to respiration, pulsation and involuntary movements as shown in Fig. 1 (top) (the corresponding dynamic sequence can be viewed at <https://youtu.be/TWq34TFGNcU>). These movements induce pixel displacements in and around the kidney region, leading to motion artefacts (intensity fluctuations) in the time–intensity curves produced from a fixed region of

interest (ROI) placed within the kidney. Such motion artefacts can affect the assessment of the kidney function.

In order to correct for such motion, many rigid and non-rigid image registration techniques have been proposed in the literature [13,37] for providing well-aligned features across the image sequence. However, developing a registration technique specific to DCE-MRI data is challenging due to the rapid change of contrast agent within the DCE-MRI sequence. Traditional registration techniques are likely to fail with DCE-MRI data as similar voxels in the sequence may have variable local intensities at each sampling time. Therefore, the algorithm has to be independent of the contrast changes within the kidney.

Senneville et al.'s [29] work assumes that the kidney is a rigid body, and its shape does not change during the MRI data acquisition. For registration purposes in Senneville's work, a human expert selects a reference image from the image sequence. The expert then manually delineates the kidney region of interest (ROI), thus forming the 'template'. Using this template, the registration of the kidneys is conducted across the DCE-MRI sequence using contrast invariant similarity matching. Other methods that require human input are reported in [6,15,21,36]. Although these approaches are potentially effective, a major issue is the need for human intervention for delineating the kidney region. Other issues are reproducibility and the intrinsic bottleneck associated with the speed of processing that automation could address.

On the other hand, approaches based on matrix decomposition such as principle component analysis (PCA), independent component analysis (ICA) and robust PCA (RPCA) have also been proposed as a preprocessing step prior to image registration. Progressive principal component registration (PPCR) introduced by Melbourne et al. [17,18] is a PCA-based approach that iteratively removes misalignment from the DCE-MRI sequence while using a standard registration algorithm such as fluid registration [5]. The author's main assumption in this work is that PCA captures contrast changes or intensity fluctuations in the first few principal components and motion in the last principal components (when sorted according to their proportion of variance explained through the cumulative sum of eigenvalues). However, using PCA for motion compensation depends purely upon the nature of the motion, i.e. for example, periodic motion of free breathing can appear in the first few principal components along with contrast changes.

In order to deal robustly with various breathing protocols, robust data decomposition registration (RDDR) [9] was introduced. RDDR uses robust principal component analysis (RPCA) [4] coupled with a registration algorithm based on residual complexity minimisation [20]. RPCA decomposes the DCE-MRI data into a series of low-rank and sparse components separating motion components from the contrast enhanced. The intensity fluctuations which remain

unchanged are then registered. The explicit separation of sparse components provide RPCA a greater degree of robustness when compared to a regular PCA-based approach. The ICA-based approach has also been used to decompose DCE-MRI data prior to registration in free breathing cardiac MRI [35]. In all of the aforementioned approaches, the main objective is to remove motion elements from the DCE-MRI time series while utilising image registration methods.

Spatio-temporal ICA (STICA) [10,30] is one method that does not use any kind of registration procedure in its approach. According to STICA's assumptions, free breathing, which induces the movement artefacts, is regarded as one of the independent processes, i.e. different regions in DCE-MRI that respond differently with respect to the contrast agent are assumed to be spatially independent, and are assumed to be temporally independent of each other [10]. Quantitative assessment in [10] using ROI analysis shows virtually no movement in either the first independent component or the second. The third independent component shows the movement artefacts. Limitations of this approach can include finding an optimal filter that can maximise the statistical independence of the these DCE signals over space and time simultaneously.

1.1 Motivation: dynamic mode decomposition (DMD)

DMD was originally introduced in the area of computational fluid dynamics (CFD) [28], specifically for analysing the sequential image data generated by nonlinear complex fluid flows [25–27,34]. The DMD decomposes a given image sequence into several images, called dynamic modes. These modes essentially capture different large-scale to small-scale structures (sparse components) including a background structure (low-rank model) [7]. DMD has gained significant applications in various fields [2,3,16], including for detecting spoof samples from facial authentication video data sets [33] and for detecting spoofed finger-vein images [31]. The advantage of this method is its ability to identify regions of dominant motion in an image sequence in a completely data-driven manner without relying on any prior assumptions about the patterns of behaviour within the data. Therefore, it is thus potentially well-suited to analyse a wide variation of blood flow and filtration patterns seen in renography pathology.

1.2 Comparison with decomposition-based methods

The assumptions of our approach are borrowed from PCCR and RDDR methods. Similar to STICA our proposed WR-DMD technique is also an image registration-free approach. Comparisons with the aforementioned decomposition-based methods are made in Table 1.

Table 1 Comparison of proposed methods with other movement correction approaches that are based on matrix decomposition methods

References	Method	Matrix Factorisation	Registration	Assumptions	Demerits/merits
Melbourne et al. [17, 18]	Progressive principal component registration (PPCR)	PCA	Multi-resolution FFD [19]	Contrast changes captured in the first few principal components and motion in the last principal components	Limitations in handling periodic motion of free breathing. Computationally expensive for using registration algorithm
Hamy et al. [9]	Robust data decomposition registration (RDDR)	RPCA	Residual complexity minimisation [20]	Sparse components separate motion components from the contrast-enhanced images	Computationally expensive. Nevertheless robust to various breathing protocols
Kiani et al. [10]	Online—STICA	ICA	None	Different regions in DCE-MRI respond differently, over the time are assumed to be independent	Computationally expensive for optimising filters that can maximise the statistical independence
Proposed method	WR-DMD	DMD	None	Sparse components separate motion components from the contrast-enhanced images. Contrast changes captured in the most significant dynamic modes and motion in the least significant	W-DMD disentangles periodic free breathing. DMD separates motion components in least significant modes. R-DMD reconstructs perfectly aligned sequence with the most significant modes. Computationally inexpensive

1.3 Our approach

Our approach is a two-step process (Fig. 2), where at first the DCE-MRI sequence is processed through window-DMD method [31] to compensate for the pseudo-periodic breathing motion (the importance of running W-DMD as a first step process is shown in Sect. 4.4). The windowed version of DMD method (here, $W = 3$) runs over three consecutive images (since motion is periodic for every three images as evaluated in Sect. 4.2) in an overlapping fashion as shown in Fig. 3.

The output of DMD at each window produces two images namely W-DMD component-1 (C1) revealing the low-rank image and W-DMD component-2 (C2) revealing the sparse component. At this stage of our approach, we discard the sparse components, i.e. W-DMD(C2)’s to compensate the pseudo-periodic free breathing motion from the DCE-MRI sequence. Second, we proceed with giving W-DMD component-1’s as an input to standard DMD algorithm, which decomposes the W-DMD(C1) sequence into several images called dynamic modes (see, Fig. 8). The dynamic contrast changes are captured in the most significant modes, and motion components are captured in the least significant modes. Using the first three significant DMD modes, the original sequence is then reconstructed via R-DMD method. Our result in Fig. 1 (bottom) shows that the motion artefacts are

compensated in an exemplar 4D dynamic medical imaging application.

1.4 Contributions

Our implementation is novel in the sense that it uses windowed-DMD on dynamic image sequences for the first time to compensate for motion artefacts by producing low-rank images as W-DMD component-1. Even though the low-rank and sparse representations of an image sequence have been reported for DMD [7, 12], the method that we propose here is essentially different. In [7], the authors exploit the low-rank and sparse representation within each frame. Specifically, low rank revealing the background and sparse presenting the foreground of that particular frame. Recently, in [12] DMD with a multi-resolution approach (MR-DMD) decomposed video streams into multi-time scale features and objects. The MR-DMD approach is similar to that of applying standard DMD technique at several resolutions after discarding the slow varying modes (background modes or the most significant modes). In other words, the MR-DMD approach runs the standard DMD algorithm over a sequence of images to produce several dynamic modes. Later, the most significant modes (background modes) are discarded; therefore, DMD is run using the least significant modes. This process is continued at several time resolutions allowing an image sequence to be separated for objects moving at different

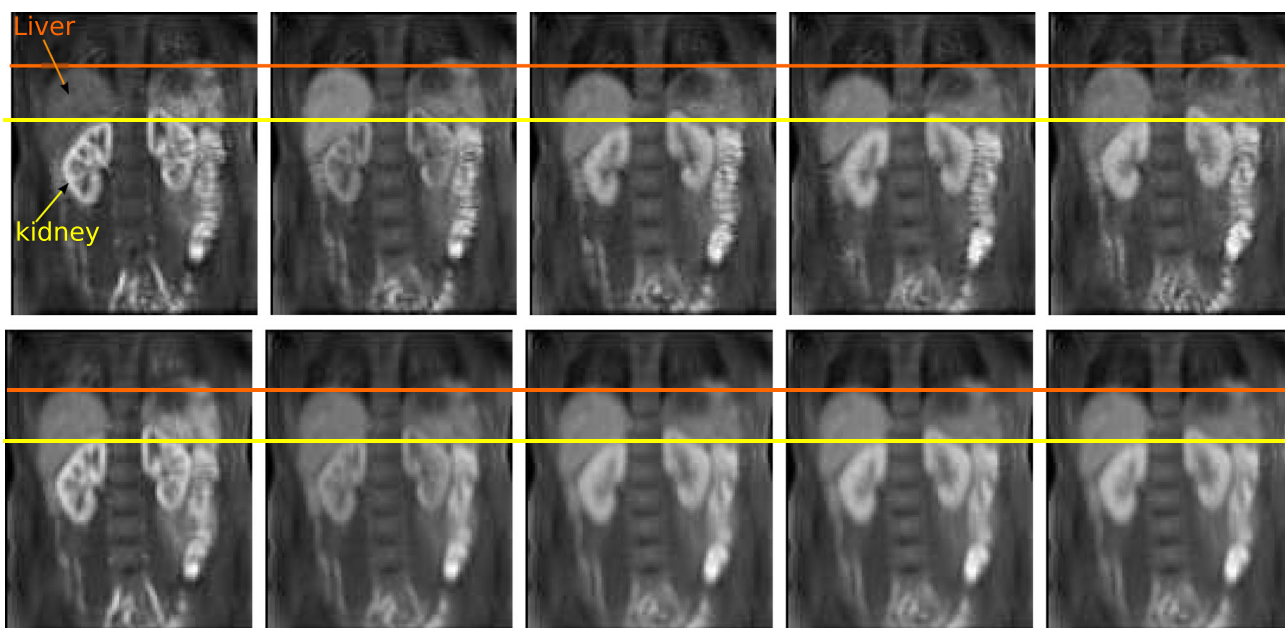


Fig. 1 (Top) 5 frames at time = {30,50,74,82,100}s selected from a DCE-MRI sequence of a healthy volunteer. The yellow and red reference lines show the alignment of the kidney and liver regions. The first image shows the peak stage of contrast agent inside the kidney region. The regions of kidney and liver clearly depict the translation of movements in the vertical direction, arising due to the patient move-

ments. (Bottom) The yellow and red reference lines clearly showing the proper alignment of the kidney and liver regions after processing with WR-DMD. The video-based results can be viewed at <https://youtu.be/TWq34TFGNcU> and <https://youtu.be/UT7f4ch4H-I> (colour figure online)

rates against the slowly varying background. This approach, therefore, allows for multiple target tracking and detection. In contrast, the proposed W-DMD method runs standard DMD over a window of consecutive images; thus producing low-rank and sparse modes at each window of the image sequence, respectively, giving rise to W-DMD component-1 and component-2. The original DMD method introduced in [28] extracts modes from a sequence of images and interprets modes in the image space, whereas our reconstruction variant of the method (R-DMD) re-projects the DMD modes back into original image sequence, thereby stabilising the complex movements. Therefore, our contributions in this study are in (i) introducing the WR-DMD framework for the first time to reconstruct movement corrected, aligned images sequence. (ii) Validating our technique using medical data with applications to DCE-MRI; and (iii) improving the understanding of the application through WR-DMD framework.

1.5 Organisation of the paper

The remainder of this paper is organised as follows: in Sect. 2, we consider the theory for WR-DMD. Sect. 3 presents 10 different data sets used in this study. In Sect. 4, we present our experiments and results, and finally, conclusions are drawn in Sect. 5.

2 Methodology

In this section, we present our methodological pipeline which consists of W-DMD and reconstruction-based DMD. The overall process framework is shown in Fig. 2 and discussed in Sect. 1.3.

2.1 Dynamic mode decomposition (DMD)

Let \bar{x}_r be the r th dynamic image frame in a DCE-MRI sequence, whose size is $m \times n$. This image frame \bar{x}_r is converted to $mn \times 1$ column vector, resulting in the construction of a data matrix \mathbf{X} of size $mn \times N$ for N image frames.

$$\mathbf{X} = [\bar{x}_1, \bar{x}_2, \bar{x}_3, \dots, \bar{x}_N] = \begin{pmatrix} x_1^1 & x_2^1 & \dots & x_N^1 \\ \vdots & \vdots & \vdots & \vdots \\ x_1^{mn} & x_2^{mn} & \dots & x_N^{mn} \end{pmatrix}. \quad (1)$$

The images in the DCE-MRI data are collected over regularly spaced time intervals, and hence, each pair of consecutive images are correlated. It can be justified that a mapping A exists between them forming a span of krylow subspace [11, 22, 23]:

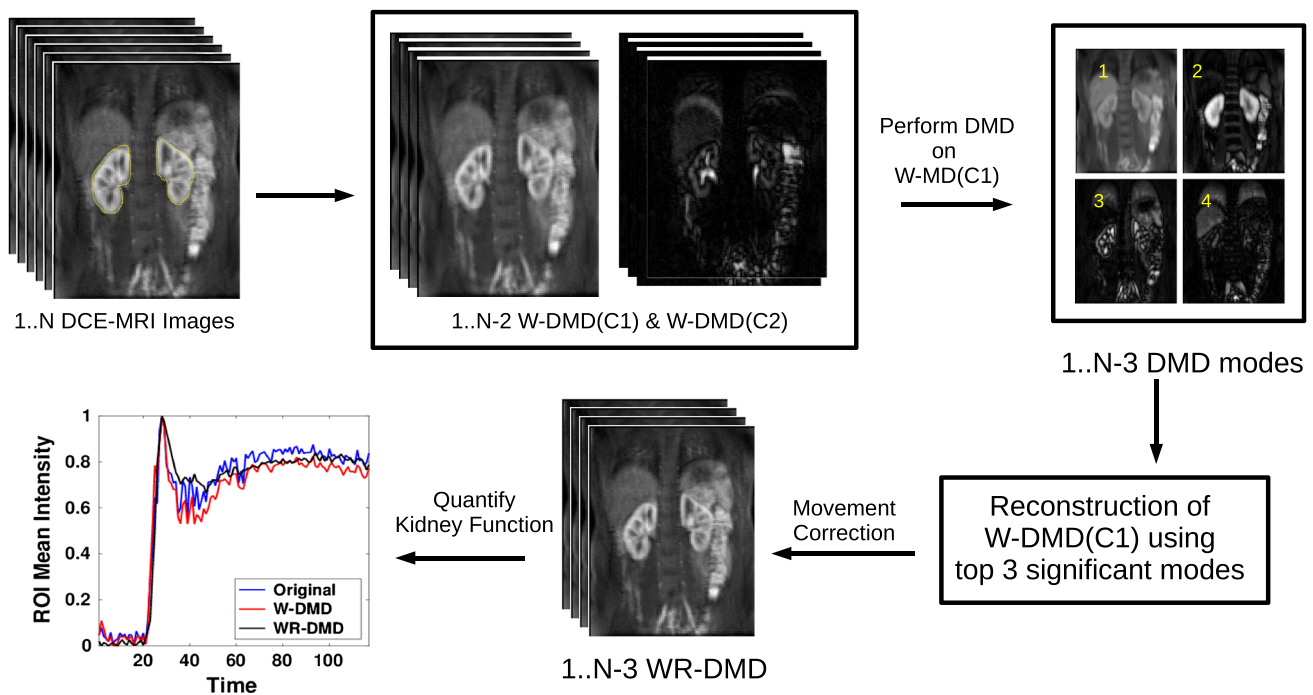


Fig. 2 Flow chart showing the steps involved in the methodological framework. First, a DCE-MRI sequence consisting of N images is processed using the W-DMD algorithm in order to output each $N - 2$ W-DMD components C1 and C2. At this stage, the W-DMD(C1) pro-

duces the low-rank images and W-DMD(C2) produces sparse images. W-DMD(C1) is given as an input to DMD which produces $N - 3$ DMD modes. The first three DMD modes are then selected for reconstructing the motion-stabilised image sequence

$$\begin{aligned} \mathbf{X} &= [\bar{\mathbf{x}}_1, A\bar{\mathbf{x}}_1, A^2\bar{\mathbf{x}}_1, A^3\bar{\mathbf{x}}_1, \dots, A^{N-1}\bar{\mathbf{x}}_1]. \\ [\bar{\mathbf{x}}_2, \bar{\mathbf{x}}_3, \dots, \bar{\mathbf{x}}_N] &= A[\bar{\mathbf{x}}_1, \bar{\mathbf{x}}_2, \dots, \bar{\mathbf{x}}_{N-1}]. \\ \mathbf{P}_2 &= A\mathbf{P}_1 + \mathbf{r}\mathbf{e}_{N-1}^T. \end{aligned} \quad (2)$$

Here, \mathbf{r} is the vector of residuals that accounts for behaviours that cannot be described completely by \mathbf{A} , $\mathbf{e}_{N-1} = \{0, 0, 1\} \in \mathcal{R}^{N-1}$, $\mathbf{P}_2 = [\bar{\mathbf{x}}_2, \bar{\mathbf{x}}_3, \dots, \bar{\mathbf{x}}_N]$ and $\mathbf{P}_1 = [\bar{\mathbf{x}}_1, \bar{\mathbf{x}}_2, \dots, \bar{\mathbf{x}}_{N-1}]$. The system \mathbf{A} is unknown and it captures the overall dynamics within the dynamic image sequence in terms of the eigenvalues and eigenvectors of \mathbf{A} , which are referred to as the DMD eigenvalues and DMD modes, respectively.

The sizes of the matrices \mathbf{P}_2 and \mathbf{P}_1 are both $mn \times N - 1$ each. Therefore, the size of unknown matrix \mathbf{A} would be $mn \times mn$. Since matrix \mathbf{A} captures the dynamical information within the image sequence, solving it provides us with the dynamics captured in the image sequence in terms of modes. Unfortunately, solving for \mathbf{A} is computationally very expensive due to its size. For instance, if an image has a size of 240×320 , i.e. $m = 240$ and $n = 320$, the size of \mathbf{A} is then 76800×76800 .

From the literature, there are two approaches for obtaining these eigenvalues and modes. The first is Arnoldi-based approach, which is useful for theoretical analysis due to its connection with Krylov subspace methods [11, 22, 23].

The second is a singular value decomposition (SVD)-based approach that is more robust to noise in the data and to numerical errors [25].

Therefore, SVD can be directly applied on \mathbf{P}_1 in Eq. (2), to obtain \mathbf{U} , $\mathbf{\Sigma}$ and \mathbf{V}^* matrices.

$$\mathbf{P}_2 = A\mathbf{U}\mathbf{\Sigma}\mathbf{V}^*. \quad (3)$$

$$\because \mathbf{P}_1 = \sum_{i=1}^d \Sigma_i \mathbf{u}_i \mathbf{v}_i^*,$$

here, Σ_i is the i th singular value of \mathbf{P}_1 , \mathbf{u}_i and \mathbf{v}_i^* are the corresponding left and right singular vectors, respectively; and d is the total number of singular values.

Re-arranging Eq. (3), we obtain the full-rank matrix \mathbf{A} ,

$$\mathbf{A} = \mathbf{P}_2 \mathbf{V} \mathbf{\Sigma}^{-1} \mathbf{U}^*. \quad (4)$$

Since the eigenvalue analysis is agnostic to any linear projection, solving the eigen problem of $\tilde{\mathbf{H}}$ is easier than that of solving for \mathbf{A} directly. Moreover, the associated eigenvectors of $\tilde{\mathbf{H}}$ provide the coefficients for the linear combination that is necessary to express the dynamics within the time-series basis.

$$\tilde{\mathbf{H}}\omega = \sigma\omega, \quad (5)$$

where ω are the eigenvectors and σ a diagonal matrix containing the corresponding eigenvalues of $\tilde{\mathbf{H}}$ matrix. The eigenvalues of $\tilde{\mathbf{H}}$ approximate some of the eigenvalues of the full system \mathbf{A} [8], and we then have:

$$\begin{aligned} \mathbf{A}\mathbf{U} &\approx \mathbf{U}\tilde{\mathbf{H}}, \\ \mathbf{A}\mathbf{U} &\approx \mathbf{U}\omega\sigma\omega^{-1}, \\ \mathbf{A}(\mathbf{U}\omega) &\approx (\mathbf{U}\omega)\sigma. \end{aligned} \tag{6}$$

Therefore, $\tilde{\mathbf{H}}$ is determined on the subspace spanned by the orthogonal singular basis vectors \mathbf{U} obtained via \mathbf{P}_1 ,

$$\begin{aligned} \tilde{\mathbf{H}} &= \mathbf{U}^*(\mathbf{A})\mathbf{U}, \\ \tilde{\mathbf{H}} &= \mathbf{U}^* (\mathbf{P}_2\mathbf{V}\Sigma^{-1}\mathbf{U}^*) \mathbf{U}, \end{aligned} \tag{7}$$

which can be rewritten as:

$$\tilde{\mathbf{H}} = \mathbf{U}^*\mathbf{P}_2\mathbf{V}\Sigma^{-1}. \tag{8}$$

Here, $\mathbf{U}^* \in \mathbb{C}^{(N-1) \times mn}$ and $\mathbf{V} \in \mathbb{C}^{(N-1) \times (N-1)}$ are the conjugate transpose of \mathbf{U} and \mathbf{V}^* , respectively; and $\Sigma^{-1} \in \mathbb{C}^{(N-1) \times (N-1)}$ denotes the inverse of the singular values Σ . By replacing $\Psi = \mathbf{U}\omega$ in Eq. (6), i.e. $\mathbf{A}(\Psi) \approx (\Psi)\sigma$, we obtain the dynamic modes Ψ . $\therefore \mathbf{U} = \mathbf{P}_2\mathbf{V}\Sigma^{-1}$; therefore, we have:

$$\Psi = \mathbf{P}_2\mathbf{V}\Sigma^{-1}\omega \tag{9}$$

The complex eigenvalues σ contain growth/decay rates and frequencies of the corresponding DMD modes [26,27]. If σ_j are the diagonal elements of σ from Eq. (5), the temporal behaviour of the DMD modes is then formed via Vandermonde matrix \mathcal{V} , which raises its column vector to the appropriate power. $\mathcal{V}(f)$ with $(N - 1) \times (f + 1)$ elements will be defined as follows:

$$\mathcal{V}(f) = \begin{pmatrix} 1 & \sigma_1^1 & \sigma_1^2 & \dots & \sigma_1^f \\ 1 & \sigma_2^1 & \sigma_2^2 & \dots & \sigma_2^f \\ \vdots & \vdots & \vdots & \vdots & \vdots \\ 1 & \sigma_{N-1}^1 & \sigma_{N-1}^2 & \dots & \sigma_{N-1}^f \end{pmatrix}, \tag{10}$$

$\mathcal{V}(N)$ is a standard Vandermonde matrix for reconstruction but if $f > N$, this is used for forecasting. DMD modes with frequencies μ_j is defined by:

$$\mu_j = \frac{\ln(\sigma_j)}{\delta t}, \tag{11}$$

where δt is the lag between the images. The real part of μ_j regulates the growth or decay of the DMD modes, while the imaginary part of μ_j drives oscillations in the DMD modes.

2.2 Ordering dynamic modes

In order to select the most significant dynamic modes, the method suggested in [7,12] is to calculate the logarithmic values of the $diag(\sigma)$. The frequencies which are near origin are the most significant modes. The other way we propose here is by calculating the phase-angles for the complex eigenvalues.

The absolute value for the phase-angles are calculated and modes with unique phase-angles are selected. Doing this will remove one of the conjugate pairs in the dynamic modes. These conjugate modes have same phase-angles but with different signs and look and capture similar information [24]. After discarding one of the conjugate pairs, the dynamic modes are then sorted in ascending order of their phase-angles. The resultant dynamic modes are thus sorted according to their significance. In this study, we have considered the first three significant dynamic modes when reconstructing the original sequence.

2.3 Reconstruction from DMD modes (R-DMD)

The novel reconstruction DMD aims at reconstructing the image sequence from the dynamic modes. This can be achieved in a least squares solution.

$$\|\Psi - \hat{\mathbf{P}}_2\mathbf{V}\Sigma^{-1}\omega\| \tag{12}$$

Therefore, the reconstruction of the original image sequence can be formulated as follows:

$$\hat{\mathbf{P}}_2 = \Psi\omega^{-1}\Sigma\mathbf{V}^{-1} \tag{13}$$

Since the contrast changes are captured in the most significant modes and motion components in the least significant ones, it is desirable to discard the least significant modes. The crux of making this work is to select the K modes that are contributing to the contrast changes, and not the motion changes.

The original sequence is thus constructed using first k significant modes along with their corresponding eigenvectors from $\tilde{\mathbf{H}}$. The algorithmic details of our approach is described in Algorithm 1.

$$\hat{\mathbf{P}}_2 = \Psi_{\{1..k\}}\omega_{\{1..k\}}^{-1}\Sigma\mathbf{V}^{-1} \tag{14}$$

2.4 Windowed-DMD (W-DMD)

The Windowed version of DMD method runs DMD over a window of consecutive images in a sequence in an overlapping fashion. The output of DMD at each window produces $W - 1$ dynamic modes where W is the length of the window. To compensate the periodic free breathing from the

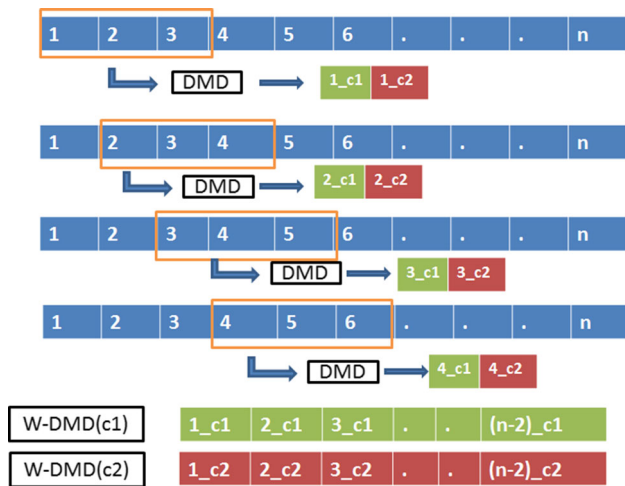


Fig. 3 Methodological pipeline showing the working mechanism of W-DMD. DMD runs over the window containing first three images in the sequence, obtaining two dynamic modes. The first dynamic mode ‘c1’ capturing the low-rank image across the window and second dynamic mode c2 capturing the sparse representation. The next step exclude the first image and consider images {2, 3, 4}, followed by {3, 4, 5} and {4, 5, 6} producing c1 and c2 components. Finally, all of the c1s and c2s across all the windows are concatenated to obtain W-DMD component-1 (W-DMD (C1)) and W-DMD component-2 (W-DMD (C2))

DCE-MRI sequence in this study, we consider $W = 3$. For instance, running DMD on the window containing the first three images in the sequence, we obtain two dynamic modes (in general for N images, we get $N - 1$ DMD modes [33]). The first dynamic mode ‘c1’ captures the low-rank image across the window and the second dynamic mode ‘c2’ captures the sparse representation, which essentially contain motion artefacts pertaining to periodic free breathing. In the next step, we exclude the first image and consider images {2, 3, 4}, followed by {3, 4, 5} and {4, 5, 6} and so on as shown in Fig. 3. Finally, we concatenate all of the c1s across all the windows to obtain W-DMD component-1 (W-DMD (C1)), and similarly, concatenation of the c2s produce W-DMD component-2 (W-DMD (C2)) [31].

Algorithm 1 WR-DMD

```

Input: Sequence of images in DCE-MRI data  $\mathbf{P} = [p_1, p_2, p_3, \dots, p_N]$ 
Output: Movement corrected sequence  $\mathbf{C}_1^2 = [c_4, c_5, c_6, \dots, c_N]$ 
1: for  $\{i = 1 \text{ to } n - w - 1\}$  #  $w = 3$ 
2:  $S = [p_i, p_{i+1}, p_{i+2}]$ 
3: [WDMD(C1)(i), WDMD(C2)(i)] = get-WDMD(S)
4: endfor
5:  $C1_1 \leftarrow [c_1, c_2, c_3, \dots, c_{N-1}]$  # C1 represents W-DMD component-1.
6:  $C1_2 \leftarrow [c_2, c_3, c_4, \dots, c_N]$ 
7:  $[U \ S \ V] \leftarrow \text{SVD}(C1_1, 'econ')$ 
8:  $\tilde{H} \leftarrow (U^* C1_2 V \Sigma^{-1})$ 
9:  $[\omega \ \sigma] \leftarrow \text{eig}(\tilde{H})$  #  $\omega$  and  $\sigma$  are the eigenvectors and eigenvalues.
10:  $\lambda_j \leftarrow \text{sort}(\text{angle}(\sigma_{jj}) >= 0)$  # sort  $\omega$  correspondingly
11:  $\Psi \leftarrow \text{abs}(P_2 V \Sigma^{-1} \omega)$  # Calculate dynamic modes
12:  $C1_2 \leftarrow (\Psi \omega^{-1} \Sigma V^{-1})$  # reconstruction
    
```

2.5 Comparisons with DMD and MR-DMD

Dynamic mode decomposition (DMD), in computer vision, has been introduced for robustly separating video frames into a background model and foreground components [7]. The DMD method has been applied on a data matrix containing image sequence from a surveillance video. The DMD eigenvalue frequencies near the origin are interpreted as background (slow varying modes) portions of the given image sequence, and the frequencies bounded away from the origin are their sparse counterparts (fast varying modes). Specifically, the parts in image sequence that do not change in time have an associated frequency $\|\mu_j\| \approx 0$, which corresponds to background.

DMD with a multi-resolution [12] approach decomposes an image sequence into multi-time scale features and objects. The MR-DMD approach is similar to that of applying standard DMD technique at several resolutions on fast varying dynamic modes after discarding the background modes or the slow varying modes. Thereby allowing an image sequence to be separated into objects moving at different rates against the slowly varying background, thus allowing for multiple target tracking and detection. MR-DMD method has efficiently demonstrated, shifting *El Niño* from ocean temperature data.

The MR-DMD framework implicitly has a windowing architecture since it implements the standard DMD on the windows of fast varying modes iteratively. In contrast, our proposed method is essentially different. Our proposed W-DMD method runs standard DMD over an overlapping window of consecutive images producing low-rank and sparse modes at each window of the image sequence. The consecutive set of low-rank images forms the W-DMD component-1 (C1), whereas W-DMD component-2 (C2) reveals the sparse components. The pseudo-periodic free breathing motion from the DCE-MRI sequence is thus compensated by discarding the sparse components, i.e. W-DMD(C2).

Later, this W-DMD (C1) is given as an input to standard DMD algorithm to produce set of most significant modes (slow varying) capturing the contrast changes, and least significant modes (fast varying modes) capturing motion components. Using the first three significant DMD modes, the original sequence is then reconstructed via our R-DMD method. Thus, utilising the pipeline of W-DMD and R-DMD we introduce WR-DMD for the first time to carry out movement correction in medical image sequences in a manner that is both extremely efficient and completely data driven.

3 Data set

The data sets obtained were from 10 healthy volunteers’ as shown in Fig. 4 acquired after injection of 0.05 mmol/kg

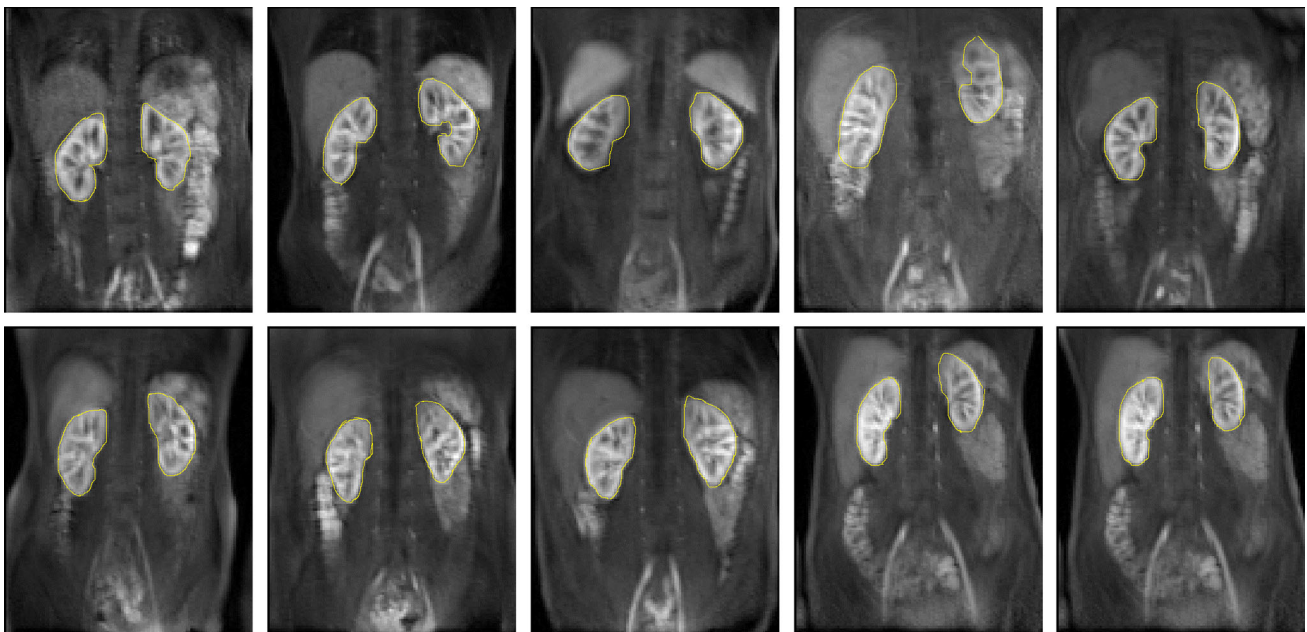


Fig. 4 Exemplars of dynamic MR images from 10 healthy volunteers' kidney slice produced by DCE-MRI sequence considered as 10 different data sets in this study. The images here show the central kidney slice at time 120s aortic peak enhancement after the contrast agent is

injected. The yellow boundary on the kidneys is a result of manual delineation from a human expert. The mean intensity values are calculated in this region across the time producing time–intensity plots (colour figure online)

of Gd-DTPA (Magnevist) contrast agent, on a 1.5T Siemens Avanto MRI scanner, using a 32-channel body-phased array coil. The MRI acquisition sequence consisted of a 3D spoiled gradient echo sequence utilising an echo time, TE of 0.6ms, repetition time, TR of 1.6ms, and a flip angle, FA = 17 degrees with a temporal resolution of 1.5s collected for 180s. The acquired DCE-MRI data sets cover the abdominal region, enclosing left and right kidneys and abdominal aorta.

4 Experiments and results

In this section, we discuss our experimental procedure along with the results. The objectives of our experiments are as follows:

1. *Selection of optimal window length (W)* The W-DMD algorithm needs parameter W , i.e. the window length to run standard DMD. The objective of this experiment is to determine the optimal W which depends on the breathing cycle of the volunteer.
2. *Importance of W-DMD method* To show the importance of W-DMD which constitutes a simplified variant of the proposal in our two-step approach, we evaluate our results with and without using the W-DMD method. Since, the W-DMD method can compensate for the pseudo-periodic free breathing from the contrast-enhanced images by discarding sparse components, we hypothesise that without using it, the reconstruction results may contain some flickering effects. Therefore, we wish to examine whether using windowed-DMD on a sliding sequence of 3 consecutive images will really stabilise these breathing motion artefacts.
3. *Qualitative assessment of dynamic information captured by DMD* From the outset, we hypothesise that DMD can capture both large scale dynamics related to contrast changes and small-scale dynamics related to motion artefacts and noise. Therefore, we wish to examine whether these features are indeed picked up by DMD or not.
4. *Reconstruction using most significant modes* Since DMD can capture the contrast-enhanced images in the most significant dynamic modes and motion in the least significant, we hypothesise that reconstruction with the top three most significant DMD modes could provide a perfectly aligned image sequence.
5. *Effect of mode selection in the reconstruction* It is of interest to investigate the impact of the most significant dynamic modes on the generalisation performance of the stability within the image sequence. For this reason, we consider modes in $M \times 4$ as a set where M ranges from 1, ..., 16. We hypothesise that stability within the image sequence should decrease with an increasing number of modes selected for reconstruction.

6. *Comparison with other registration methods* We wish to examine the performance strength of our approach by comparing with two registration methods from the literature.

4.1 Evaluation

The evaluation of our experiments is based on two perspectives.

1. From the clinical perspective, we would like to examine the feasibility of using our approach as a means for removing respiratory motion artefacts from the dynamic image sequence containing dramatic regional changes in intensity due to contrast agent flow affecting the quality of the resulting time–intensity curves used for analysis. The curves are produced by calculating the mean intensity of the target ROI in an image, which in this case is based on the kidney. ROI analysis using time–intensity curves containing respiratory motion artefacts may affect subsequent compartmental model fitting, as the motion may also obscure subtle time–intensity features. Therefore, we have considered the smoothness of the time–intensity curve as a surrogate metric for quality of motion compensation. The smoother this curve is, the better the performance.
2. From the signal processing and computer vision perspective, we would like to examine the strength of our approach by calculating the mean motion magnitude across the DCE-MRI sequence. Since, the respiratory motion represents an obfuscating issue within the dynamic image sequence, it distracts attention away from, and potentially masks, areas that may exhibit subtle pathology within the image. For this purpose, we evaluate the motion between two consecutive images over the entirely reconstructed dynamic sequence in order to characterise the amount of motion as an indication of the stability of the dynamic sequence. This criteria is evaluated using a method called block-matching-block motion estimation [1]. A well-reconstructed dynamic sequence should have a smaller overall global mean.

4.2 Selection of optimal W (window length)

In order to determine optimal W , we would like to see whether there exists any periodicity in the motion. For this purpose, we calculate the motion amongst the images in the sequence with respect to the first image using block-matching algorithm. This algorithm estimates the motion between two images using ‘blocks’ of pixels, i.e. by matching the block of pixels in image K to a block of pixels in image K' by moving the block of pixels over a search region. The block subdivides the image K in block sizes [height width] and Overlap

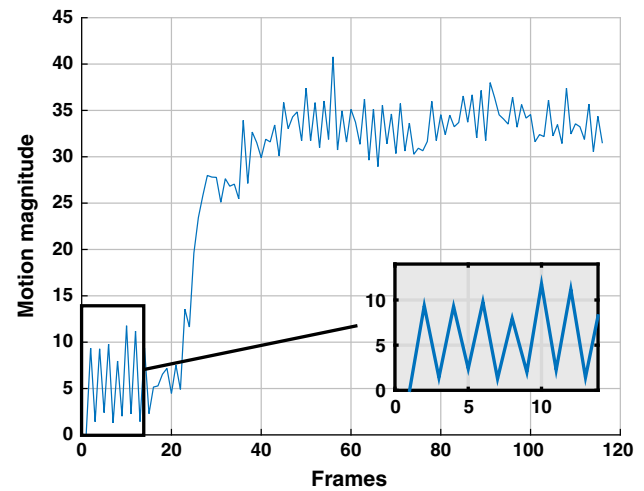


Fig. 5 Motion magnitude with respect to first image in the sequence across the data set-1

$[r\ c]$ parameters. For each subdivision or block in image K' , the algorithm establishes a search region based on the maximum displacement $[r\ c]$ parameter. The block searches for the new block location using an exhaustive search method [14]. We have considered [height, width] = [15, 15] and $[r, c]$ = [5, 5].

The motion magnitudes across the data set-1 with respect to first image of the sequence is shown in Fig. 5. It can be clearly seen that the motion is periodic for every three consecutive images. Therefore, we have chosen a window length of 3 to conduct our experiments.

4.3 Performance of W-DMD

Each of the 10 healthy volunteers’ DCE-MRI dynamic sequences consisting of 120 images are given as an input to W-DMD algorithm sequentially. The DMD algorithm at each sliding window consisting of three images produces two dynamic modes namely W-DMD component-1 revealing the low-rank image and W-DMD component-2 revealing the sparse image as shown in Fig. 6. All the low-rank images are then concatenated to form a sequence of 118 images called W-DMD component-1 (W-DMD(C1)) and similarly the concatenation of sparse images form W-DMD(C2).

For the purpose of clinically relevant evaluation, an expert (radiologist) manually delineated the kidney ROIs across the 10 data sets as shown in Fig. 4. Using these ROIs, the time–intensity curves are obtained. The curves for W-DMD(C1) for the right kidney shows a little reduction in intensity variations as seen in Fig. 7 (W-DMD (red)). The evaluation results after processing with block-matching algorithm depicts a decrease of 80.54% average motion magnitude against the original sequences across the 10 data sets as shown in Fig. 9.

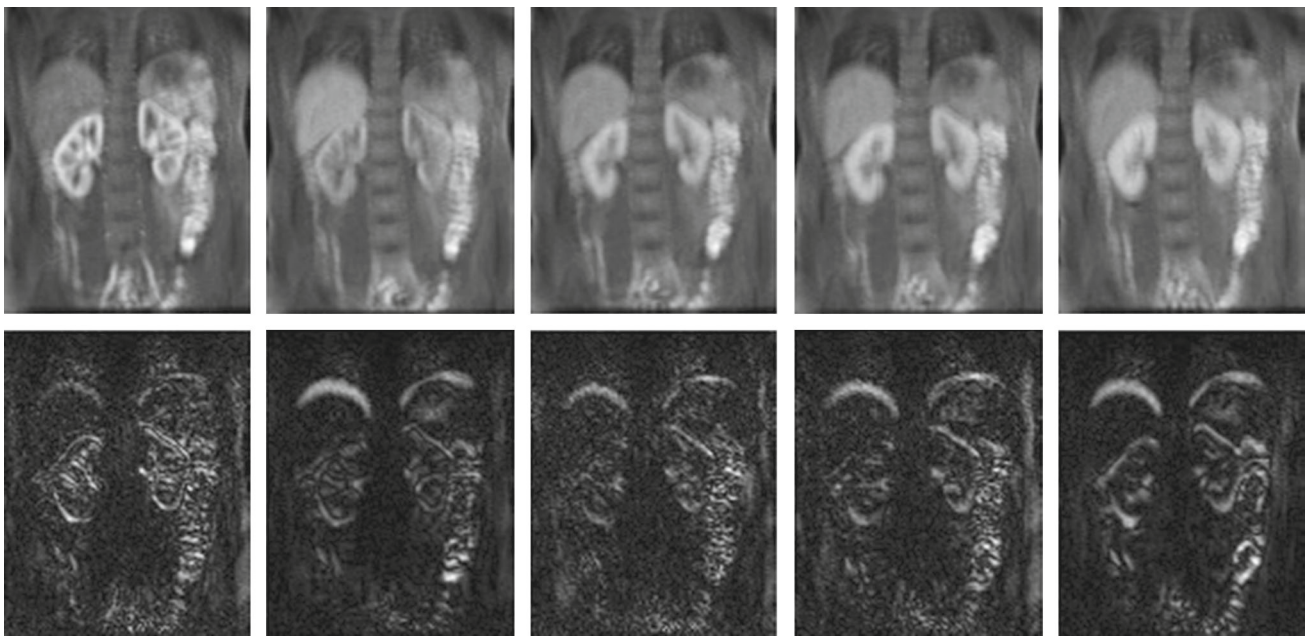


Fig. 6 (Top) five images from data set-1's W-DMD(C1) at time = {30,50,74,82,100}s showing the low-rank images. The first image shows the peak stage of contrast agent inside the kidney region. (Bottom) Corresponding images from the W-DMD(C2) showing their sparse representation

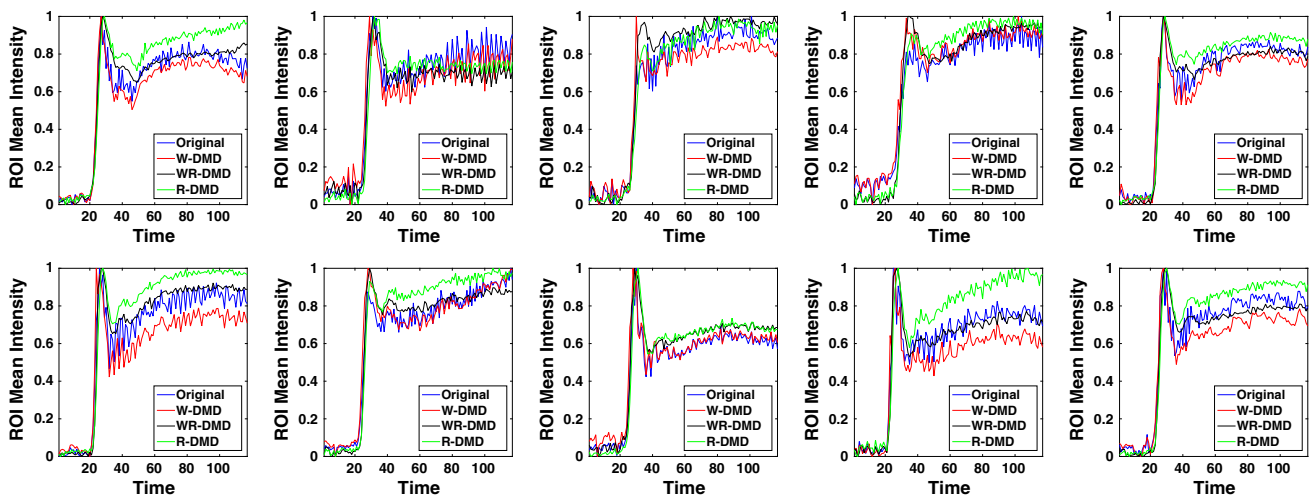


Fig. 7 Time–intensity curves across 10 data sets (sequentially from left to right)

4.4 Importance of W-DMD

In order to examine the strength of W-DMD, we directly input each of the ten healthy volunteers' DCE-MRI dynamic sequences to the standard DMD algorithm. Using the top three most significant modes, the original sequence is reconstructed using our R-DMD method. The results in Fig. 9 show greater motion magnitude when compared to results obtained through W-DMD on the data sets {1, 4, 9, 10}. The time–intensity plots in Fig. 7 from data sets {2, 3, 5, 6, 7, 9} reveal a greater amount of fluctuations from the graphs produced by the R-DMD method even though the results of

their mean motion magnitude are lower when compared to W-DMD method. This proves our hypothesis that although excluding the W-DMD step stabilises the motion globally, the periodic free breathing would still remain locally. Therefore, discarding the sparse components, i.e. W-DMD(C2) eliminates periodic free breathing from the contrast-enhanced images.

4.5 Qualitative assessment of DMD

In the next step, the W-DMD(C1) containing the low-rank images are then given as an input to DMD algorithm produc-

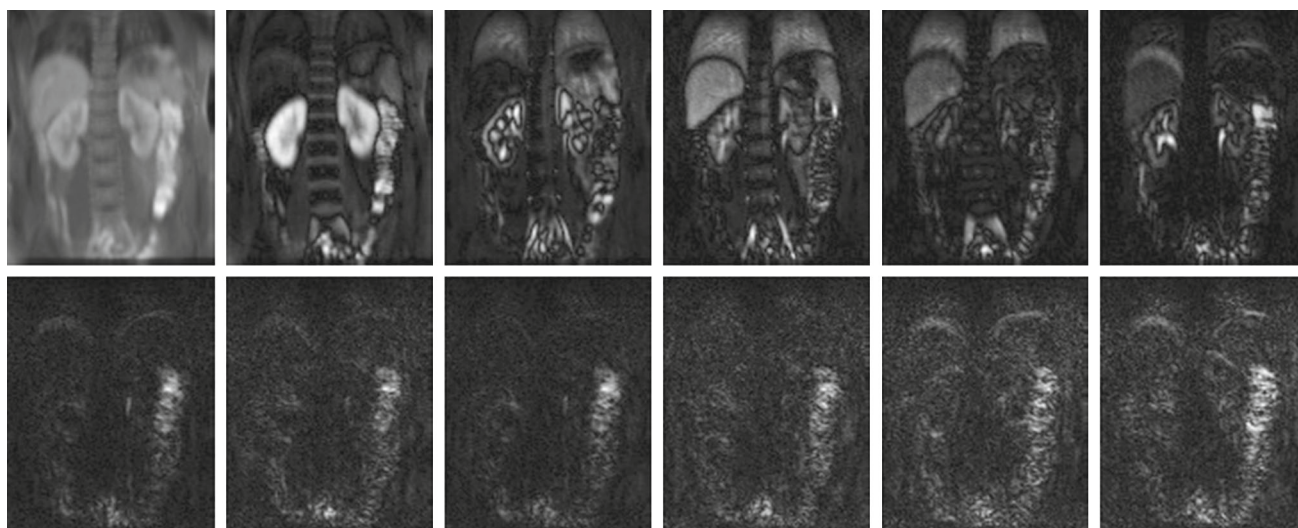


Fig. 8 (Top) The top six most significant DMD modes on W-DMD(C1) from data set-1. (Bottom) bottom six least significant DMD modes on W-DMD(C1)

ing 117 dynamic modes. The first mode reveals the low-rank model across all the images and the remaining 116 modes capture the sparse representations. The contrast changes are captured in the most significant modes, in particular, mode-2 capturing kidney region and mode-3 and 4, spleen and the liver regions, respectively, as shown in Fig. 8 (top) for data set-1.

Noise and residuals including the motion components are captured in the least significant modes [Fig. 8 (bottom)].

4.6 Reconstruction using most significant modes

The first three modes are selected for the reconstruction of the W-DMD(C1) sequence of images, discarding the rest of the 113 modes. The reconstructed W-DMD(C1) using the WR-DMD algorithm produces a very promising and stable image sequence compensating for all the complex movements. The qualitative results obtained from the WR-DMD (black) in Fig. 7 show smoother curves in the time–intensity plots when compared to the original sequence and W-DMD(C1) sequence. Complete complex movement artefacts arising due to respiration, pulsation and involuntary movements are all compensated through the WR-DMD reconstructed images as shown in Fig. 9. A decrease of 99% average motion magnitude can be seen against the original sequences across the 10 data sets.

4.7 Effect of mode selection in the reconstruction

Since reconstruction needs to operate with significant modes, it is of interest to find out the minimum number of modes required. We hypothesise that a greater number of modes should result in less stable performance; however, at the same

time, we would like to know the minimum number of modes that are required to reconstruct the original sequence. Consequently, we select the windows of the first $\{4, 8, \dots, 64\}$ images. We can consider at most 64 modes because one member of each conjugate pairs of the DMD mode is redundant. Consequently, we are left with 61–62 modes. The results in Fig. 10 reveal that as the number of modes increases, the mean motion magnitude also increases, consistent with our hypothesis that a greater number of modes results in increased motion variance (methodologically, we would expect the optimal number of DMD modes to be data dependent).

4.8 Comparison with other registration methods

In order to compare our approach with registration-based methods, we should follow a gold standard approach that is manually delineating the target region and performing the rigid registration, which requires a human expert and is inconvenient. Nevertheless, to obtain a fair comparison, a human expert manually delineated the area around the right kidney region. Therefore, we have selected only this part of the delineated region for the registration and not the whole image. We have opted to use intensity-based methods such as Affine and translation registration methods for our comparison, since these methods are less sensitive to contrast change, and their implementation is freely available.

Evaluating the performance of our approach on DCE-MRI data is difficult due to the lack of the prior knowledge on contrast change and the motion.

One way of evaluating the performance is to calculate the total variation score given by the estimate of the standard deviation of the consecutive m time–intensity data points $\hat{t}_{[i]} \forall i \in \{1, \dots, m\}$. Smaller values indicate smoother time

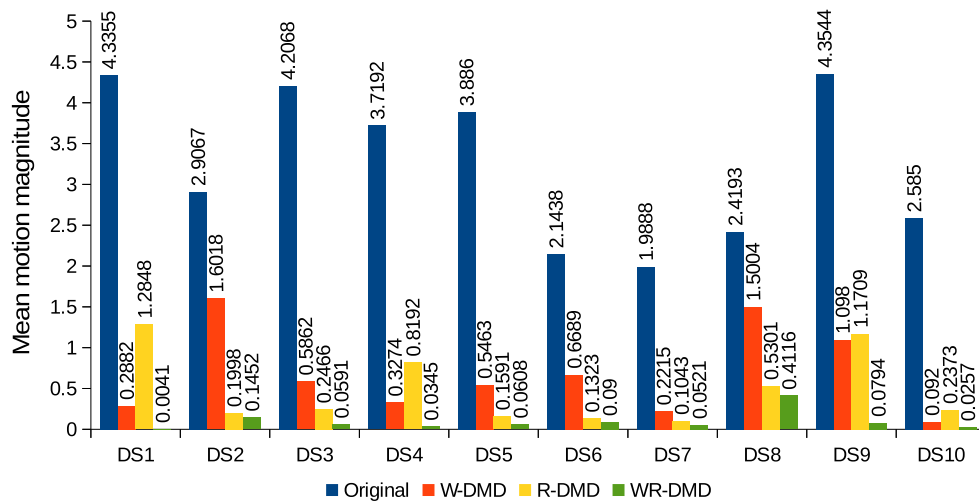


Fig. 9 A comparison of mean motion magnitude between original and W-DMD-, R-DMD- and WR-DMD-processed image sequences. The results are shown across 10 data sets calculated using block-matching-block algorithm. A smaller mean motion magnitude indicates a more stable sequence

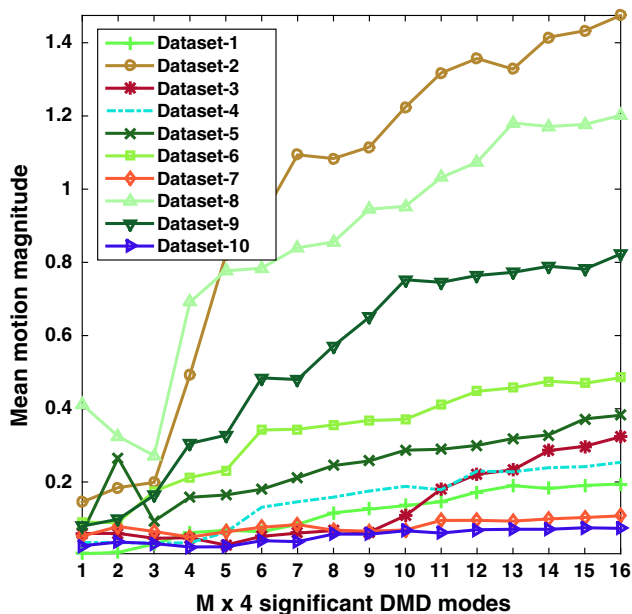


Fig. 10 Mean motion magnitude across 10 data sets calculated using block-matching-block algorithm utilising WR-DMD. A smaller mean motion magnitude indicates a more stable sequence. Here, M is the number of modes that were used in the reconstruction process. As the number of modes increases, the mean motion magnitude also increases

series. However, this is scale variant and depends upon the application. Therefore, to induce scale invariance, we evaluate the ‘degree of smoothness’ score of the total variation score calculated from the time–intensity data points by dividing it by the absolute mean of the difference of the consecutive time intensity data points. The difference is used to avoid the assumption of stationarity in the data and it is calculated as $\tilde{\mathbf{t}}_{[i]} \leftarrow \hat{\mathbf{t}}_{[i+1]} - \hat{\mathbf{t}}_{[i]}, \forall i \in \{1, \dots, m\}$.

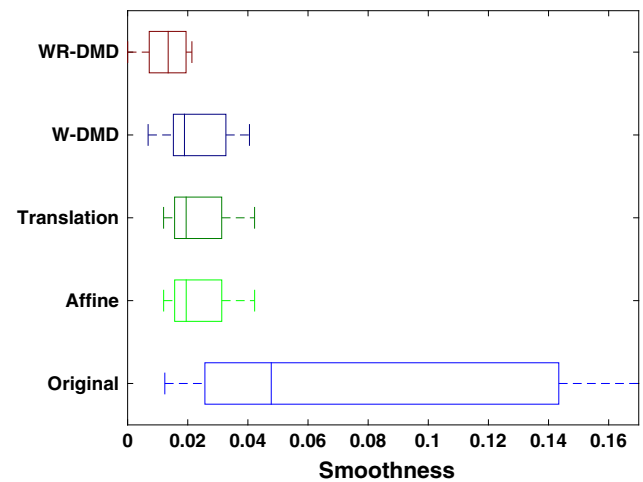


Fig. 11 Comparison with intensity-based image registration methods. Each box-plot has 10 values corresponding to 10 data sets. A smaller value in the X-axis indicates greater smoothness; so smaller is better

The degree of smoothness score \mathbf{D} is thus given by:

$$\mathbf{D} = \frac{std(\tilde{\mathbf{t}})}{abs(mean(\tilde{\mathbf{t}}))}. \quad (15)$$

The results in Fig. 11 clearly show WR-DMD outperforms the standard registration methods.

5 Conclusions, discussions and future directions

This study shows the significance of WR-DMD approach, as a viable movement correction algorithm for processing DCE-MRI data. We applied the WR-DMD approach on 10

data sets of DCE-MRI data collected from healthy volunteers. The proposed algorithm has very low time complexity¹. In addition, compared to existing methods, e.g. RDDR & STICA, it has the advantage of requiring no parameter tuning. W-DMD can extract low-rank and sparse representations within an image sequence. The motion artefacts for periodic free breathing are captured in the sparse components. The low-rank W-DMD component-1 is then given as an input to the standard DMD algorithm producing dynamic modes. We found that the contrast changes are captured in the most significant dynamic modes and motion in the least significant ones. The original sequence is then reconstructed utilising the top three most significant dynamic modes using R-DMD. The results demonstrate that the proposed WR-DMD method is a promising approach for correcting respiratory or similar motions in complex dynamic medical image sequences containing significant temporal intensity changes due to contrast agent uptake or other comparable mechanisms.

The major point of discussion would be in answering whether the WR-DMD framework be sufficiently robust when it comes to scanning patients who tend to be more susceptible to motion artefacts? From the clinical point of view, this can only be answered with a conjecture as we have no patient data but we would argue ‘yes’ [29]. This question provides a good opportunity to recognise that both volunteers and patients will be susceptible to motion. From computer vision and signal processing point of view, W-DMD, in this study has been demonstrated for removing pseudo-periodic breathing motion. It is always necessary to check whether there exists any pseudo-periodic breathing in the data set. For this purpose, motion amongst the images in the sequence with respect to the first image should be calculated using block-matching algorithm as discussed in Sect. 4.2. Later, the number of images for which the motion is periodic should be determined. For example, in Sect. 4.2 we show that the motion was periodic for every three images in our data sets, and hence, we set $W=3$ as a parameter in W-DMD to conduct our experiments. Similarly if the periodicity in the motion is observed for ‘ n ’ images for a patient/ healthy volunteer, especially children, who tend to be more susceptible to motion artefacts, we conjecture that making the window length adaptive to ‘ n ’ might be sufficient to tackle the pseudo-periodic motion.

The adaptive version of the W-DMD forms our future work. In addition to that, DMD, in this study, also has demonstrated to extract dominating regions of causally-connected intensity fluctuations. In this context, perfusion inside the kidney region is the most dominating region with the intensity fluctuations due to the injection of contrast agent. DMD

was thus able to naturally capture the kidney region as mode-2 followed by liver and spleen in the other modes. Therefore, in our future work we would like to perform segmentation of the kidney region of interest for automatically quantifying the kidney function. Finally, we would like to explore the possibility of using our proposed methodology in automatically correcting for the movements in ‘coloured’ [32] aerial images which are captured of the same terrain but on different days.

Acknowledgements The funding for this work has been provided by the Department of Computer Science and the Centre for Vision, Speech and Signal Processing (CVSSP)—University of Surrey. ‘I.G’ would like to express gratitude towards Kidney Research, UK, for funding the DCE-MRI data acquisition as part of a reproducibility study. ‘S.T’ and ‘N.P’ have benefited from the Medical Research Council (MRC) funded project ‘Modelling the Progression of Chronic Kidney Disease’ under the grant number R/M023281/1. The details of the project are available at www.modellingCKD.org. ‘D.W’ acknowledges the financial support from the Horizon 2020 European Research project ‘DREAMS4CARS’ (#731593).

Open Access This article is distributed under the terms of the Creative Commons Attribution 4.0 International License (<http://creativecommons.org/licenses/by/4.0/>), which permits unrestricted use, distribution, and reproduction in any medium, provided you give appropriate credit to the original author(s) and the source, provide a link to the Creative Commons license, and indicate if changes were made.

References

1. Barjatya, A.: Block matching algorithms for motion estimation. *IEEE Trans. Evolut. Comput.* **8**(3), 225–239 (2004)
2. Berger, E., Sastuba, M., Vogt, D., Jung, B., Amor, H.B.: Dynamic mode decomposition for perturbation estimation in human robot interaction. In: *The 23rd IEEE International Symposium on Robot and Human Interactive Communication*, pp. 593–600 (2014). doi:[10.1109/ROMAN.2014.6926317](https://doi.org/10.1109/ROMAN.2014.6926317)
3. Brunton, B.W., Johnson, L.A., Ojemann, J.G., Kutz, J.N.: Extracting spatial–temporal coherent patterns in large-scale neural recordings using dynamic mode decomposition. *J. Neurosci. Methods* **258**, 1–15 (2016)
4. Candès, E.J., Li, X., Ma, Y., Wright, J.: Robust principal component analysis? *J. ACM (JACM)* **58**(3), 11 (2011)
5. Crum, W., Tanner, C., Hawkes, D.: Anisotropic multi-scale fluid registration: evaluation in magnetic resonance breast imaging. *Phys. Med. Biol.* **50**(21), 5153 (2005)
6. Gerig, G., Kikinis, R., Kuoni, W., von Schulthess, G.K., Kübler, O.: Semiautomated roi analysis in dynamic MR studies. Part I: image analysis tools for automatic correction of organ displacements. *J. Comput. Assist. Tomogr.* **15**(5), 725–732 (1991)
7. Grosek, J., Kutz, J.N.: Dynamic mode decomposition for real-time background/foreground separation in video. *arXiv preprint arXiv:1404.7592* (2014)
8. Grosek, J., Kutz, J.N.: Dynamic mode decomposition for real-time background/foreground separation in video. *CoRR arXiv:abs/1404.7592* (2014)
9. Hamy, V., Dikaivos, N., Punwani, S., Melbourne, A., Latifoltogjar, A., Makanyanga, J., Chouhan, M., Helbren, E., Menys, A., Taylor, S., et al.: Respiratory motion correction in dynamic mri

¹ That is, image sequence containing 120 frames each of size 120×104 takes about 3–5 s to compute on a desktop computer with 8GB of RAM memory running Intel(R) Core(TM) i5-4590 CPU @ 3.30GHz.

- using robust data decomposition registration-application to dcmri. *Med. Image Anal.* **18**(2), 301–313 (2014)
10. Kiani, S., Gordon, I., Windridge, D., Wells, K.: On-line spatio-temporal independent component analysis for motion correction in renal dce-mri. In: *Nuclear Science Symposium and Medical Imaging Conference (NSS/MIC)*, 2012 IEEE, pp. 2910–2915. IEEE (2012)
 11. Krylov, A.: On the numerical solution of the equation by which in technical questions frequencies of small oscillations of material systems are determined. *Izvestija AN SSSR (News of Academy of Sciences of the USSR)*, Otdel. mat. i estest. nauk **7**(4), 491–539 (1931)
 12. Kutz, J.N., Fu, X., Brunton, S.L.: Multiresolution dynamic mode decomposition. *SIAM J. Appl. Dyn. Syst.* **15**(2), 713–735 (2016)
 13. Lee, V.S., Rusinek, H., Noz, M.E., Lee, P., Raghavan, M., Kramer, E.L.: Dynamic three-dimensional mr renography for the measurement of single kidney function: Initial experience 1. *Radiology* **227**(1), 289–294 (2003)
 14. Li, R., Zeng, B., Liou, M.L.: A new three-step search algorithm for block motion estimation. *IEEE Trans. Circuits Syst. Video Technol.* **4**(4), 438–442 (1994)
 15. Maintz, J.A., Viergever, M.A.: A survey of medical image registration. *Med. Image Anal.* **2**(1), 1–36 (1998)
 16. Mann, J., Kutz, J.N.: Dynamic mode decomposition for financial trading strategies. *Quant. Finance* **16**(11), 1643–1655 (2016)
 17. Melbourne, A., Atkinson, D., White, M., Collins, D., Leach, M., Hawkes, D.: Registration of dynamic contrast-enhanced MRI using a progressive principal component registration (ppcr). *Phys. Med. Biol.* **52**(17), 5147 (2007)
 18. Melbourne, A., Hipwell, J., Modat, M., Mertzaniidou, T., Huisman, H., Ourselin, S., Hawkes, D.: The effect of motion correction on pharmacokinetic parameter estimation in dynamic-contrast-enhanced mri. *Phys. Med. Biol.* **56**(24), 7693 (2011)
 19. Modat, M., Ridgway, G.R., Taylor, Z.A., Lehmann, M., Barnes, J., Hawkes, D.J., Fox, N.C., Ourselin, S.: Fast free-form deformation using graphics processing units. *Comput. Methods Progr. Biomed.* **98**(3), 278–284 (2010)
 20. Myronenko, A., Song, X.: Intensity-based image registration by minimizing residual complexity. *IEEE Trans. Med. Imaging* **29**(11), 1882–1891 (2010)
 21. Rogelj, P., Zoellner, F.G., Kovačič, S., Lundervold, A.: Motion correction of contrast-enhanced mri time series of kidney. In: *Proceedings of the 16th International Electrotechnical and Computer Science Conference (ERK 2007)*, Portoroz, Slovenia, pp. 191–194. Citeseer (2007)
 22. Ruhe, A.: Rational krylov sequence methods for eigenvalue computation. *Linear Algebra Appl.* **58**, 391–405 (1984)
 23. Saad, Y.: Krylov subspace methods for solving large unsymmetric linear systems. *Math. Comput.* **37**(155), 105–126 (1981)
 24. Sayadi, T., Schmid, P., Nichols, J., Moin, P.: Dynamic mode decomposition of controlled h-and k-type transitions. *Annual Research Briefs (Center for Turbulence Research)*, 2013 p. 189 (2013)
 25. Schmid, P., Li, L., Juniper, M., Pust, O.: Applications of the dynamic mode decomposition. *Theor. Comput. Fluid Dyn.* **25**(1–4), 249–259 (2011)
 26. Schmid, P.J.: Dynamic mode decomposition of numerical and experimental data. *J. Fluid Mech.* **656**, 5–28 (2010)
 27. Schmid, P.J., Meyer, K.E., Pust, O.: Dynamic mode decomposition and proper orthogonal decomposition of flow in a lid-driven cylindrical cavity. In: *8th International Symposium on Particle Image Velocimetry*, pp. 25–28 (2009)
 28. Schmid, P.J., Sesterhenn, J.L.: Dynamic mode decomposition of numerical and experimental data. In *Bull. Amer. Phys. Soc.*, 61st APS meeting, San Antonio p. 208 (2008)
 29. de Senneville, B.D., Mendichovszky, I.A., Roujol, S., Gordon, I., Moonen, C., Grenier, N.: Improvement of MRI-functional measurement with automatic movement correction in native and transplanted kidneys. *J. Magn. Reson. Imaging* **28**(4), 970–978 (2008)
 30. Stone, J., Porrill, J., Porter, N., Wilkinson, I.: Spatiotemporal independent component analysis of event-related fmri data using skewed probability density functions. *NeuroImage* **15**(2), 407–421 (2002)
 31. Tirunagari, S., Poh, N., Bober, M., Windridge, D.: Windowed dmd as a microtexture descriptor for finger vein counter-spoofing in biometrics. In: *Information Forensics and Security (WIFS)*, 2015 IEEE International Workshop on. IEEE (2015)
 32. Tirunagari, S., Poh, N., Bober, M., Windridge, D.: Can dmd obtain a scene background in color? In: *Image, Vision and Computing (ICIVC)*, International Conference on, pp. 46–50. IEEE (2016)
 33. Tirunagari, S., Poh, N., Windridge, D., Iorliam, A., Suki, N., Ho, A.T.: Detection of face spoofing using visual dynamics. *IEEE Trans. Inf. Forensics Secur.* **10**(4), 762–777 (2015)
 34. Tirunagari, S., Vuorinen, V., Kaario, O., Larmi, M.: Analysis of proper orthogonal decomposition and dynamic mode decomposition on les of subsonic jets. *CSI J. Comput.* **1**, 20–26 (2012)
 35. Wollny, G., Kellman, P., Santos, A., Ledesma-Carbayo, M.J.: Automatic motion compensation of free breathing acquired myocardial perfusion data by using independent component analysis. *Med. Image Anal.* **16**(5), 1015–1028 (2012)
 36. Zikic, D., Sourbron, S., Feng, X., Michaely, H.J., Khamene, A., Navab, N.: Automatic alignment of renal DCE-MRI image series for improvement of quantitative tracer kinetic studies. In: *Medical Imaging*, (pp. 691432–691432). International Society for Optics and Photonics (2008)
 37. Zöllner, F.G., Sance, R., Rogelj, P., Ledesma-Carbayo, M.J., Rørvik, J., Santos, A., Lundervold, A.: Assessment of 3D DCE-MRI of the kidneys using non-rigid image registration and segmentation of voxel time courses. *Comput. Med. Imaging Gr.* **33**(3), 171–181 (2009)



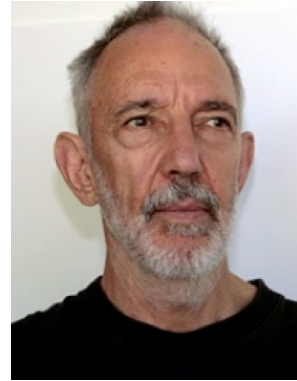
Santosh Tirunagari is Research Fellow in Computer Science at University of Surrey. His research interests centre on the fields of probabilistic machine learning, statistical signal processing and computer vision, with a former research interest in computational fluid dynamics. He obtained his PhD in computer Science from the University of Surrey in the year 2017. He has published more than 25 peer-reviewed publications and won the best research potential and the best presentation awards (PhDCompConf 2015, IEEE ICIVC 2016). He was also a session chair at IEEE SSCI held at Athens, in 2016. He is a member of IEEE as well as a member of IEEE SPS and IEEE CIS.



Norman Poh is a Senior Lecturer in the Department of Computer Science. He received the Ph.D. degree in computer science in 2006 from the Swiss Federal Institute of Technology Lausanne (EPFL), Switzerland. His work focuses on advancing pattern recognition techniques with applications to biometrics, healthcare analytics, and big data. In these areas, he has published more than 100 publications, won five award-winning papers (AVBPA05, ICB09, HSI

2010, ICPR 2010 and Pattern Recognition Journal 2006) and Researcher of the Year 2011 Award, University of Surrey. He was awarded two personal research grants from the Swiss National Science Foundation (Young Prospective Researcher Fellowship and Advanced Researcher Fellowships). He is the PI of the MRC-funded “Modelling CKD progression” (www.modellingCKD.org). He is a member of IEEE and IAPR, an IEEE Certified Biometrics Professional and trainer, and a member of the Education Committee of the IEEE Biometric Council.

standards for over 20 years, chairing the MPEG-7, CDVS and CVDA groups. Dr. Bober is an inventor of over 70 patents and several of his inventions are deployed in consumer and professional products. His publication record includes over 80 refereed publications, including three books and book chapters.



Dr. Isky Gorden is a Consultant Radiologist and Nuclear Medicine Physician with special interest in paediatric imaging. His focus has been on research into renal disease especially in children with a prenatal diagnosis of hydronephrosis. He is currently an Emeritus Professor of Paediatric Radiography at University College London, Great Ormond Street Institute of Child Health.



Kevin Wells is Reader in Medical Imaging at the Centre for Vision Speech & Signal Processing at the University of Surrey. Prior to his current academic position at Surrey, he previously worked at the Institute of Cancer Research/Royal Marsden Hospital, University College London and University of Bath. His research interests revolve around image analysis and simulation, with particular interests in respiratory motion modelling and

mammography, funded from CancerResearchUK, RC-UK, various charitable and industrial partners. He has over 140 publications, with his work being recognised via an IET Innovations award (2012), SPIE Cum Laude (2010) and SPIE Honorable Mention (2015) awards. He is a member of the Institute of Physics, a Chartered Physicist and a Chartered Engineer.



David Windridge is Reader in Computer Science at Middlesex University and heads the university’s Data Science group. His research interests centre on the fields of machine learning, cognitive systems and computer vision, with a former research interest in astrophysics (he obtained his Ph.D. in Cosmology at the University of Bristol UK). He has authored and played a leading role on a number of large-scale machine learning projects in academic and industrial

research settings (including the EPSRC ACASVA and EU DIPLECS projects). He has also won a number of interdisciplinary research grants in areas such as psychological modelling and proteomic classification. He is a Visiting Professor at Trento University, Italy, and a visiting Senior Researcher at the University of Surrey (he was previously a Senior Research Fellow within the Centre for Vision, Speech and Signal Processing). He has authored more than 80 peer-reviewed publications.



Miroslaw Bober is a professor of Video Processing at the University of Surrey, U.K. In 2011 he co-founded Visual Atoms Ltd, a start-up specializing in Visual Search Technologies. Between 1997 and 2011 he headed Mitsubishi Electric Corporate R&D Center Europe (MERCE-UK). Prof. Bober received the MSc and PhD degrees from University of Surrey, in 1991 and 1995, respectively. His research interests include various aspects of computer vision and machine

intelligence, with recent focus on image/video database retrieval and data mining. He has been actively involved in the development of MPEG